Electronic Supplementary Material (ESI) for Photochemical & Photobiological Sciences.
This journal is © The Royal Society of Chemistry and Owner Societies 2019

Dynamics and efficiency of photoswitching in biliverdin-binding phytochromes

Eleonora Consiglieri, Alexander Gutt, Wolfgang Gärtner, Luiz Schubert, Cristiano Viappiani , Stefania Abbruzzetti and Aba Losi *

*: aba.losi@unipr.it

Electronic supplementary information (ESI)

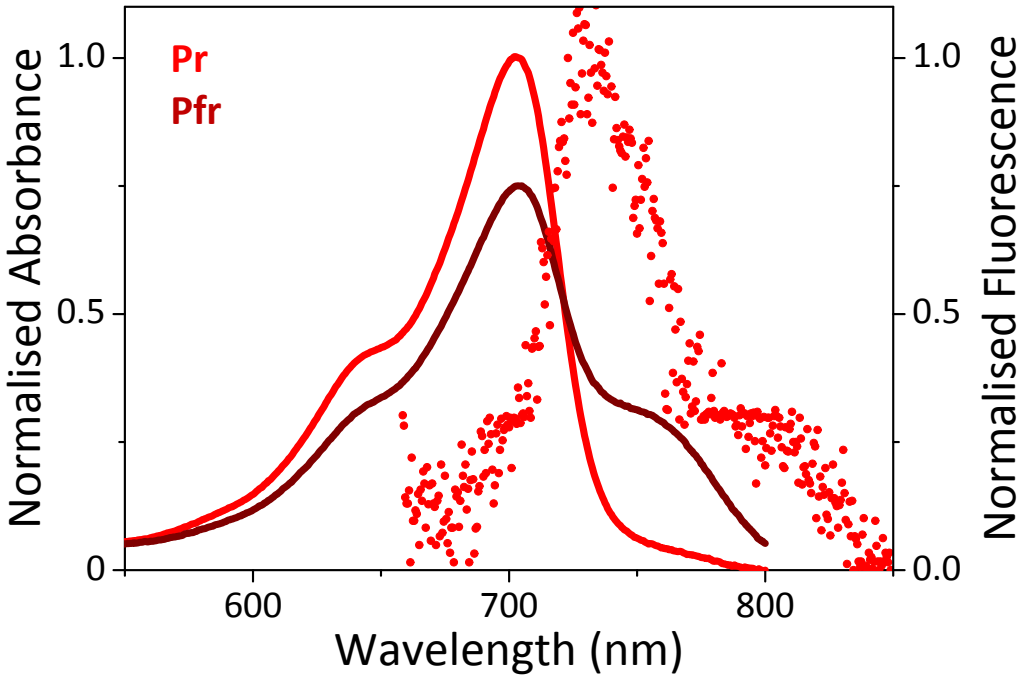

Fig. S1. Absorption and fluorescence spectra of PstBphP1 in the Pr (red) and Pfr (dark red) forms. Pfr is not fluorescent . Pr represents the dark adapted form.

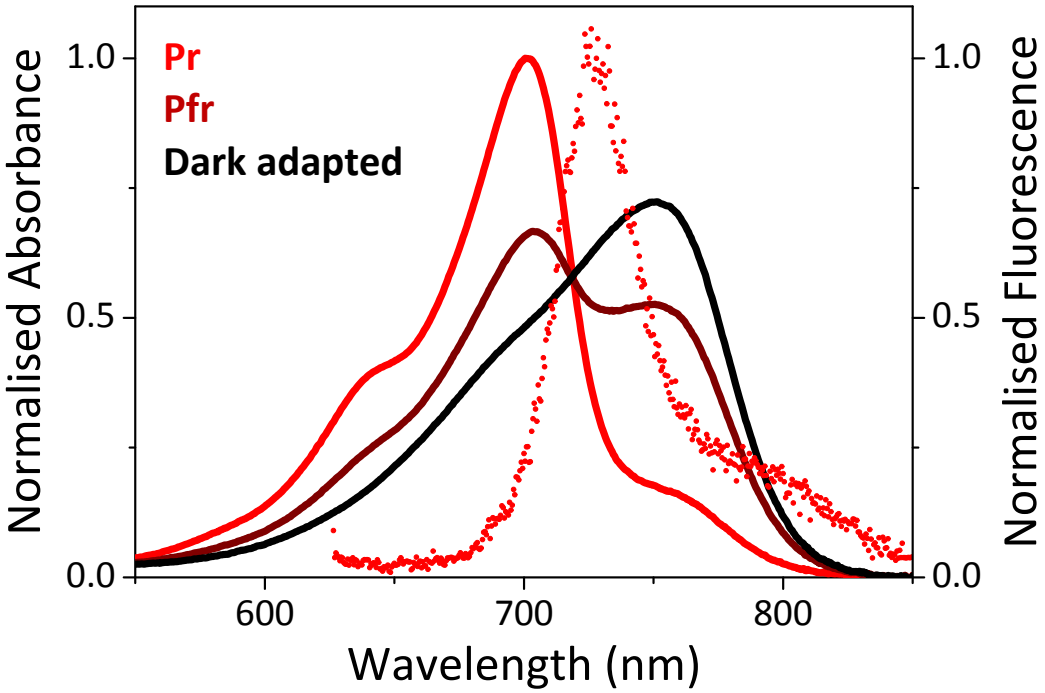

Fig. S2. Absorption and fluorescence spectra of PaBphPin the Pr (red) , darPfr (dark red) forms. The black line is the dark adapted state, = 100% Pfr. Pfr is not fluorescent

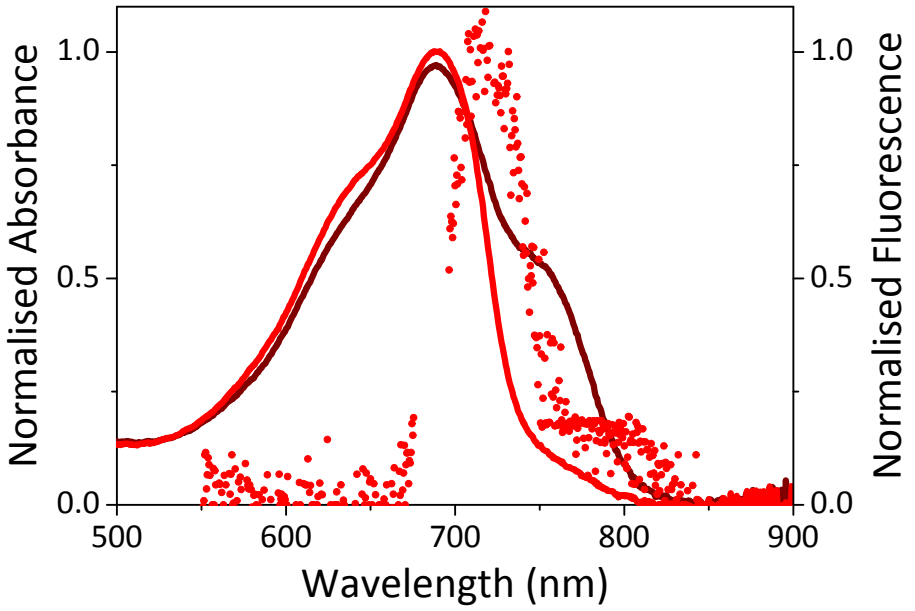

Fig. S3. Absorption and fluorescence spectra of FphAN753 in the Pr (red) and Pfr (dark red) forms. Pfr is not fluorescent . Pr represents the dark adapted form.

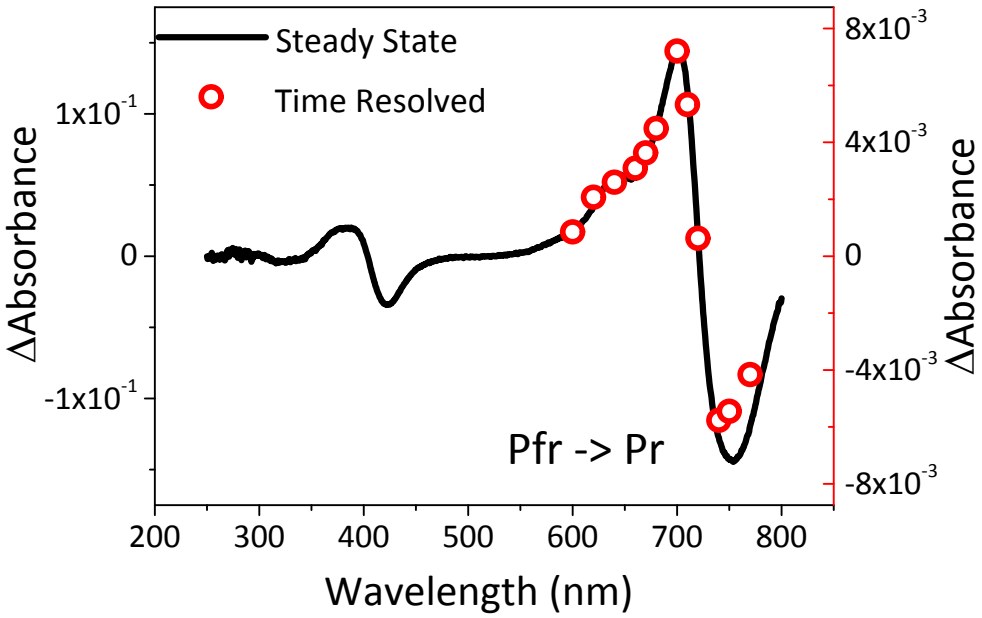

Fig. S4. Comparison of matched ΔA values for detected wavelengths to the steady state absorption difference spectrum of PstBphP1, for the Pfr-to-Pr route (pump beam wl = 760 nm). Steady state spectrum and absorption values at the end of the flash photolysis experiment (at 20 °C) are presented with difference spectrum (Pr-Pfr) . Steady state spectrum and absorption values at the end of the flash photolysis experiment (at 20 °C) are presented with different scales for the y-axes.

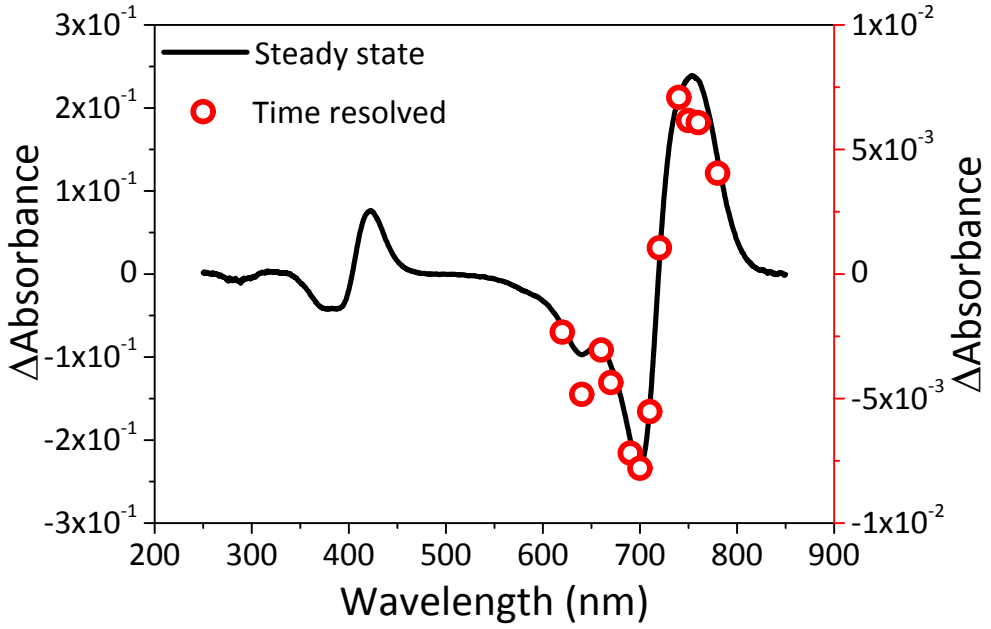

Fig. S6. Comparison of matched ΔA values for detected wavelengths to the steady state absorption difference spectrum of *Pa*BphP, for the Pr-to-Pfr route (pump beam wl = 760 nm). Steady state spectrum and absorption values at the end of the flash photolysis experiment (at 20 °C) are presented with difference spectrum (Pfr-Pr) . Steady state spectrum and absorption values at the end of the flash photolysis experiment (at 20 °C) are presented with different scales for the y-axes.

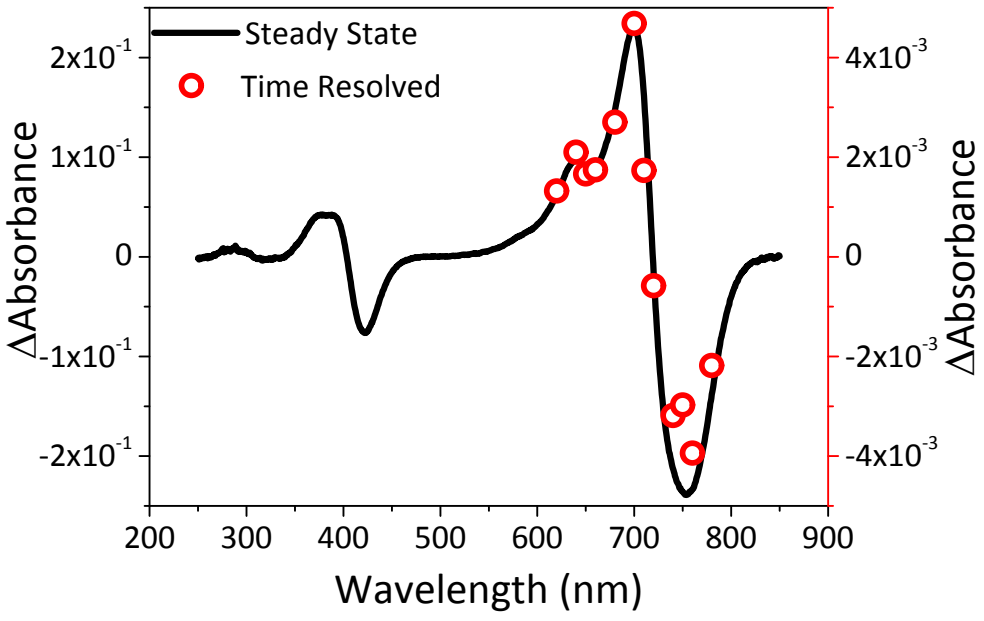

Fig. S6. Comparison of matched ΔA values for detected wavelengths to the steady state absorption difference spectrum of *Pa*BphP, for the Pfr-to-Pr route (pump beam wl = 760 nm). Steady state spectrum and absorption values at the end of the flash photolysis experiment (at 20 °C) are presented with difference spectrum (Pr-Pfr) . Steady state spectrum and absorption values at the end of the flash photolysis experiment (at 20 °C) are presented with different scales for the y-axes.

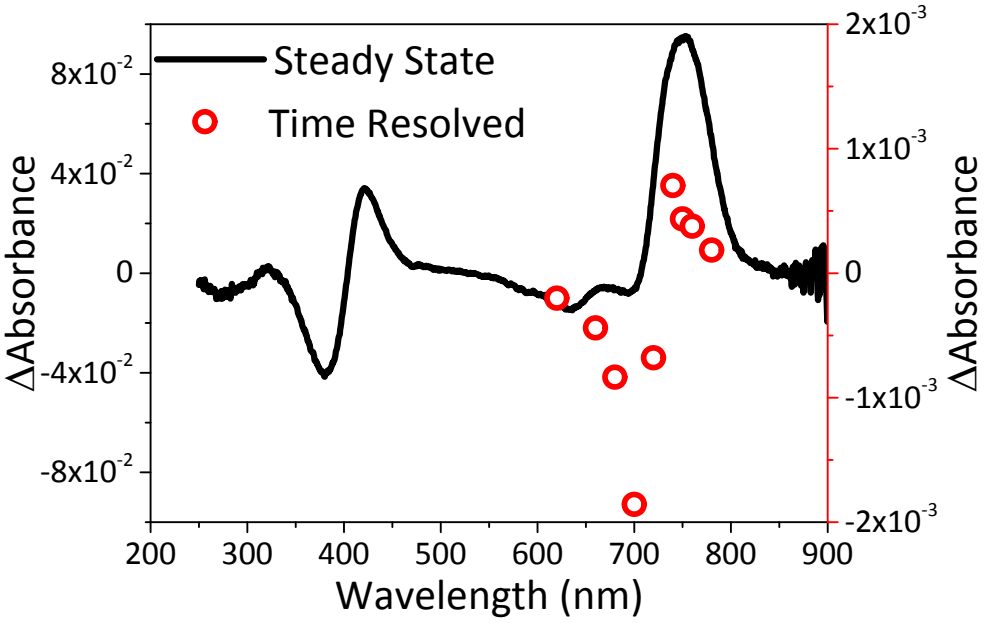

Fig. S7. Comparison of matched ΔA values for detected wavelengths to the steady state absorption difference spectrum of *F*phAN753 for the Pr-to-Pfr route (pump beam wl = 650 nm). Steady state spectrum and absorption values at the end of the flash photolysis experiment (at 20 °C) are presented with difference spectrum (Pfr-Pr) . Steady state spectrum and absorption values at the end of the flash photolysis experiment (at 20 °C) are presented with different scales for the y-axes.

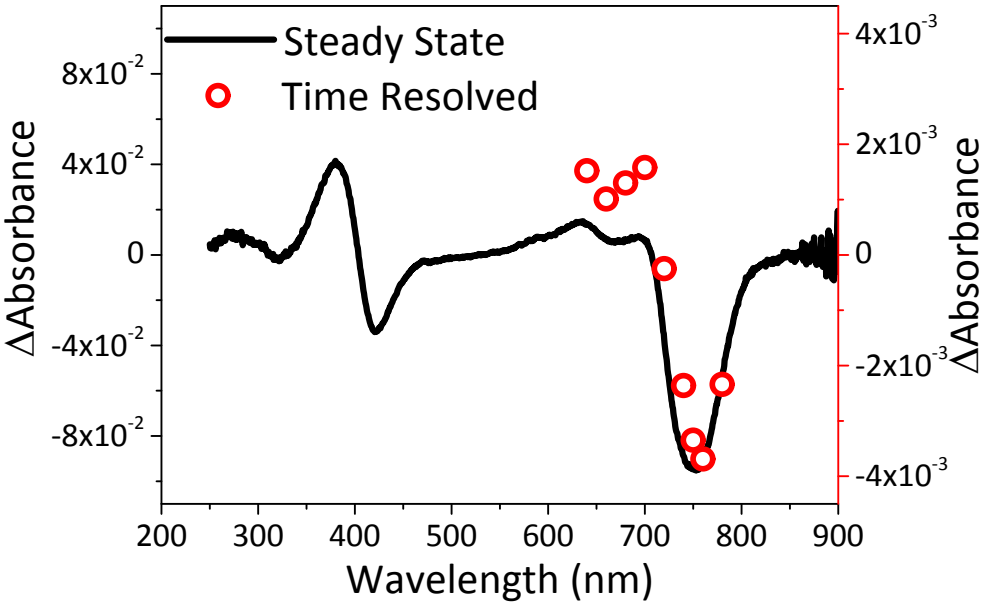

Fig. S8. Comparison of matched ΔA values for detected wavelengths to the steady state absorption difference spectrum of *F*phAN753 for the Pfr-to-Pr route (pump beam wl = 760 nm). Steady state spectrum and absorption values at the end of the flash photolysis experiment (at 20 °C) are presented with difference spectrum (Pr-Pfr) . Steady state spectrum and absorption values at the end of the flash photolysis experiment (at 20 °C) are presented with different scales for the y-axes.

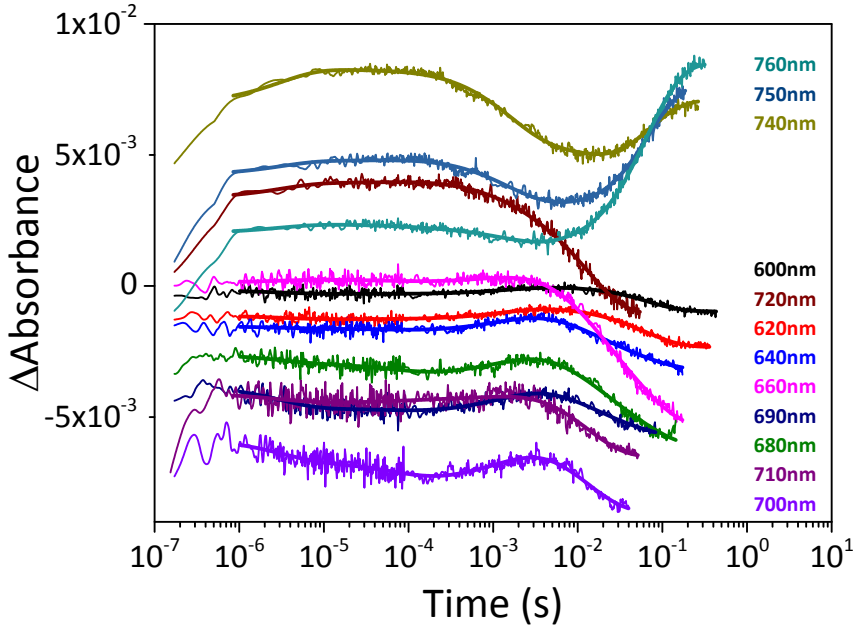

Fig. S9. Kinetics for -the Pr-to-Pfr photoconversion in *Pst*BphP1 , detected at several wavelengths; note the logarithmic time axis.

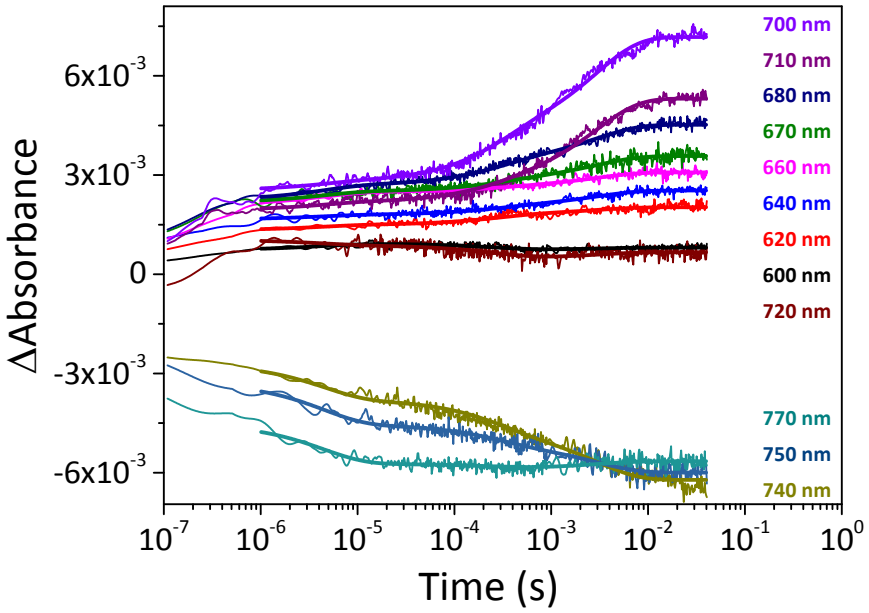

Fig. S10. Kinetics for -the Pfr-to-Pr photoconversion in *Pst*BphP1 , detected at several wavelengths; note the logarithmic time axis.

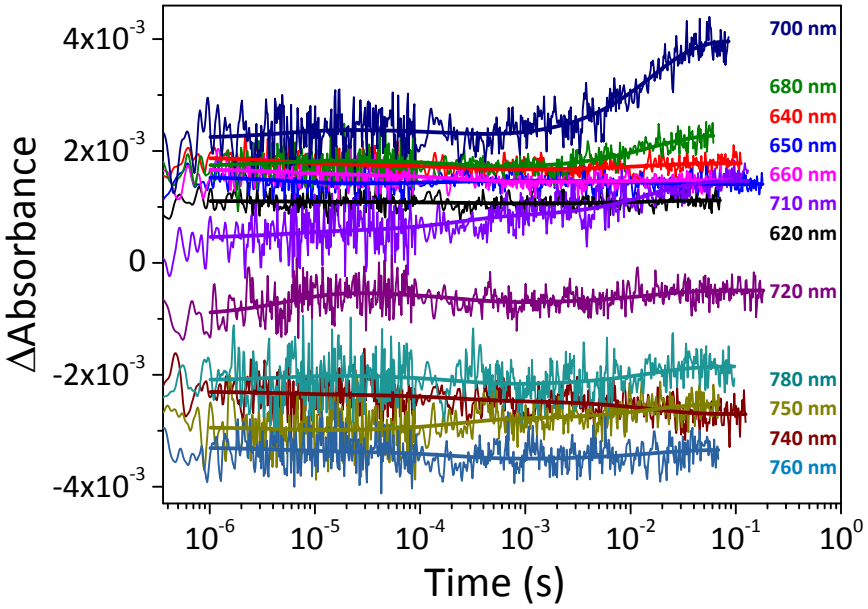

Fig. S11. Kinetics for -the Pfr-to-Pr photoconversion in *Pa*BphP , detected at several wavelengths; note the logarithmic time axis.

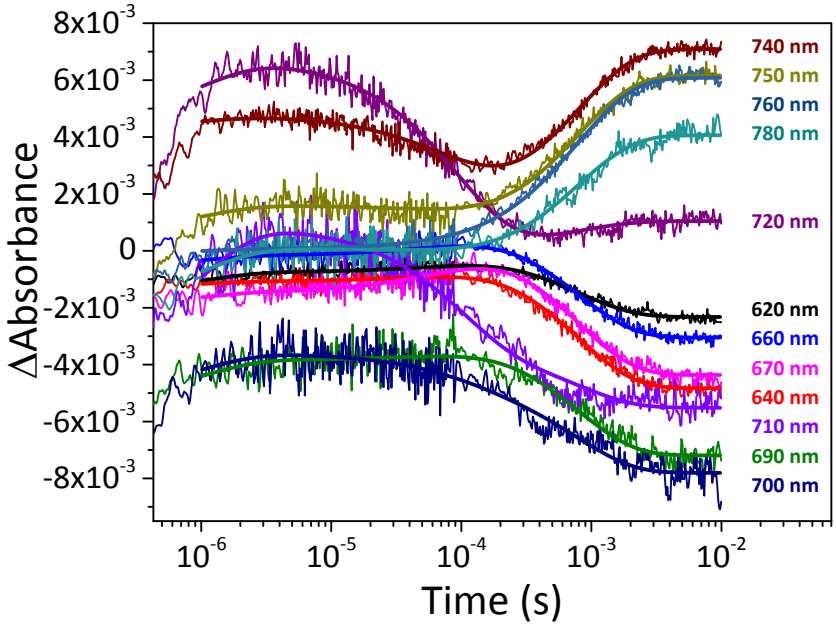

Fig. S12. Kinetics for -the Pr-to-Pfr photoconversion in *Pa*BphP , detected at several wavelengths; note the logarithmic time axis.

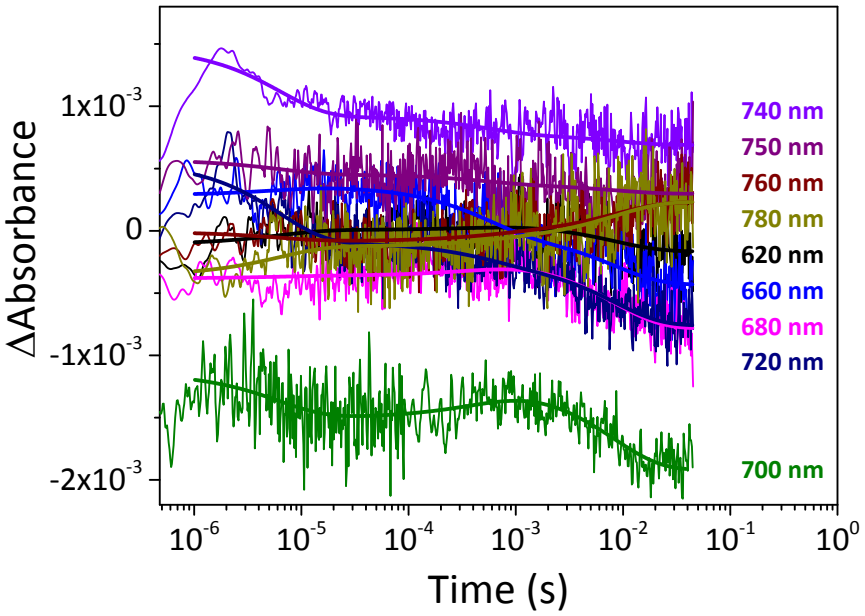

Fig. S13. Kinetics for -the Pr-to-Pfr photoconversion in FphAN753 , detected at several wavelengths; note the logarithmic time axis.

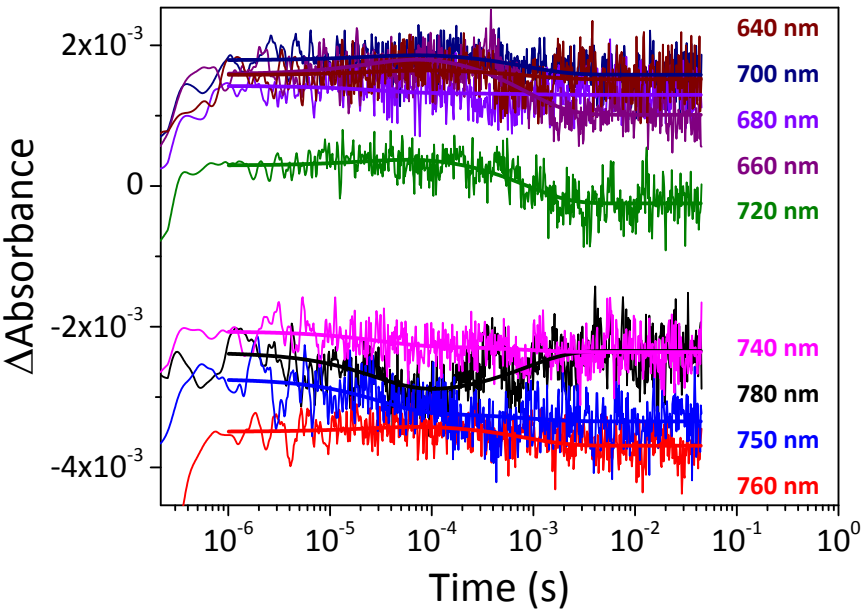

Fig. S14. Kinetics for -the Pfr-to-Pr photoconversion in FphAN753 , detected at several wavelengths; note the logarithmic time axis.

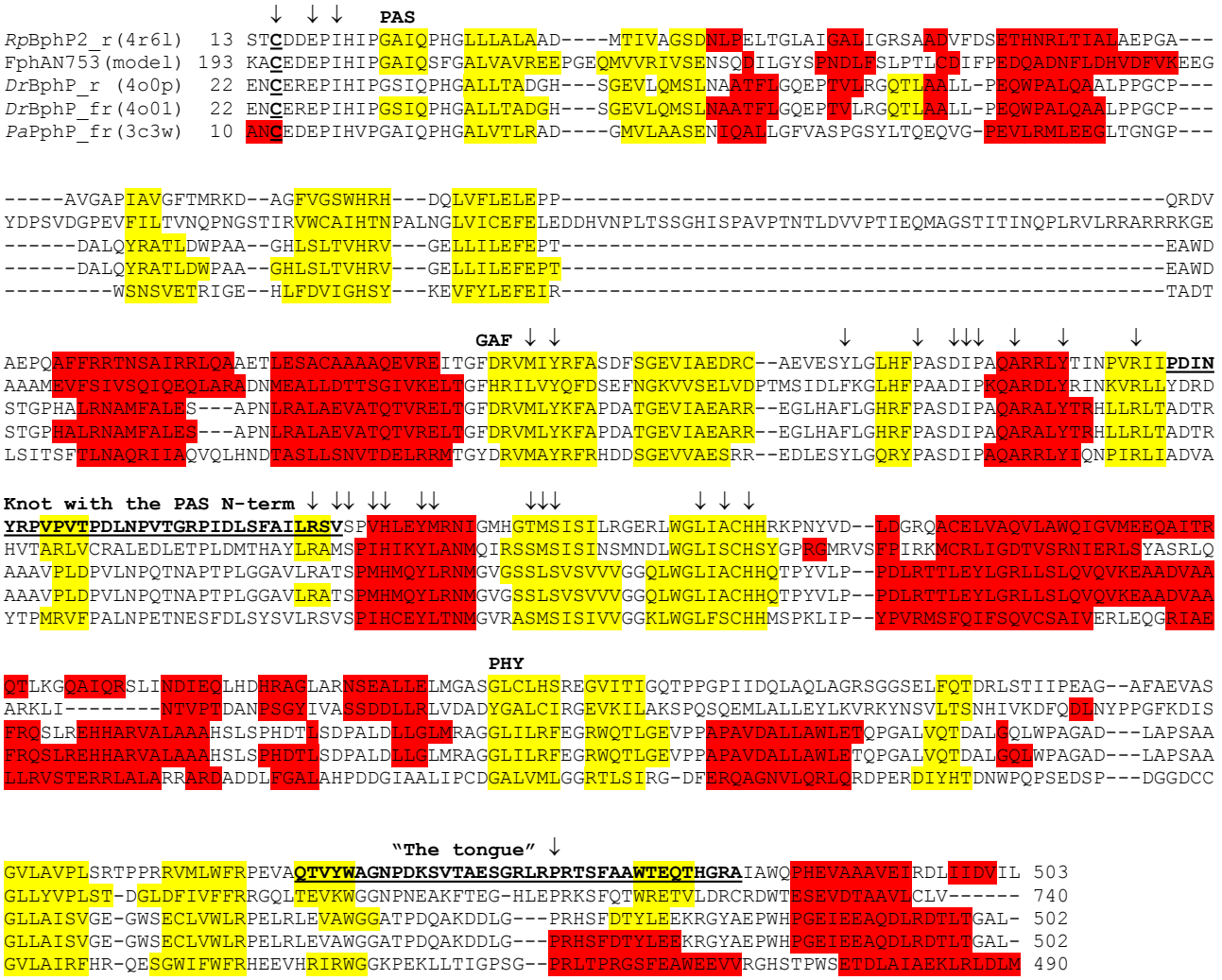

Figure S15. Sequence and secondary structure elements comparison of the photosensing PHY-GAF-PHY module for *A. nidulans* FphA with BphPs of known structure. The beginning of the core region of each domain (starting with a β-strand) is indicated with PAS, GAF and PHY. A structural homology model of FphA753 (not shown) was built with the automated mode in SWISS-MODEL,[1] using as a template the structure of *Rp*BphP2 (*Rp* = *Rhodopseudomonas palustris*) in the Pr form (Protein Data Bank, PDB, code =4R6L). The global quality of the model was quite low (GMQE, Global Model Quality Estimation, =0.58), basically due to the long insertion of 50 aa (319-368) between the PAS and the GAF domain. Single domains could be modeled as good (PAS) and eccellent (GAF and PHY). The PAS domain contain shorter, extra insertions. Important structural elements such as the "knot" and the "tongue"[2] appear to be preserved in FphA, but for the latter, in the conserved PRxSF motif,[3] phenylalanine is changed for proline. The chromophore-binding cysteine is in bold and underlined (N-terminal to the PAS core). The symbol ↓ indicates a residue in close vicinity of the chromophore (≤ 4.5 Å) in the template *Rp*BphP2. For the other sequences: *Dr* = *Deinococcus radiodurans*, *Pa* = *Pseudomonas aeruginosa*, "r" and "fr" indicate the Pr and Pfr form respectively; PDB code are indicated in parenthesis. Note that in Pfr forms one of the β-strand in the β-hairpin "tongue" is changed for an α-helix with respect to Pr states.[4]

1. M. Biasini, S. Bienert, A. Waterhouse, K. Arnold, G. Studer, T. Schmidt, F. Kiefer, T. Gallo Cassarino, M. Bertoni, L. Bordoli and T. Schwede, SWISS-MODEL: modelling protein tertiary and quaternary structure using evolutionary information., *Nucleic Acids Res.*, 2014, **42**, W252-8.

2. K. Anders and L.-O. Essen, The family of phytochrome-like photoreceptors: diverse, complex and multi-colored, but very useful, *Curr. Opin. Struct. Biol.*, 2015, **35**, 7–16.

3. L.-O. Essen, J. Mailliet and J. Hughes, The structure of a complete phytochrome sensory module in the Pr ground state., *Proc. Natl. Acad. Sci. U. S. A.*, 2008, **105**, 14709–14.

4. H. Takala, A. Björling, O. Berntsson, H. Lehtivuori, S. Niebling, M. Hoernke, I. Kosheleva, R. Henning, A. Menzel, J. A. Ihalainen and S. Westenhoff, Signal amplification and transduction in phytochrome photosensors., *Nature*, 2014, **509**, 245–248.